physica status solidi

pss

www.pss-journals.com

reprint

WILEY-VCH

Phys. Status Solidi B **252**, No. 8, 1872–1876 (2015) / **DOI** 10.1002/pssb.201451767

physica status solidi b
www.pss-b.com
basic solid state physics

Source of instability at the amorphous interface between $InGaZnO_4$ and SiO_2: A theoretical investigation

Hochul Song,[1] Youngho Kang,[1] Ho-Hyun Nahm,[,2,3] and Seungwu Han[*1]**

[1] Department of Materials Science and Engineering and Research Institute of Advanced Materials, Seoul National University, Seoul 143-747, Korea
[2] Center for Correlated Electron Systems, Institute for Basic Science (IBS), Seoul 151-747, Korea
[3] Department of Physics and Astronomy, Seoul National University, Seoul 151-747, Korea

Received 31 December 2014, revised 28 February 2015, accepted 2 March 2015
Published online 2 April 2015

Keywords density-functional theory, $InGaZnO_4$, interface, SiO_2

[*] Corresponding author: e-mail hansw@snu.ac.kr
[**] e-mail hohyunnahm@snu.ac.kr

In order to identify the source of charge trapping sites causing the device instability, we carry out *ab initio* calculations on the interface between amorphous SiO_2 and $InGaZnO_4$. The interface structure is modeled by joining the two amorphous phases with additional annealing steps. The theoretical band offset is obtained by aligning oxygen 2s levels and shows good agreement with experiment. For the stoichiometric interface, we could not identify any defects within the gap that can capture positive holes. However, when oxygen vacancies are introduced at the interface, the Si–metal bonds are formed, resulting in the defect levels within the band gap. When positively charged with holes, the Si–metal bonds undergo huge relaxations, implying that the recovery to the original neutral state should involve a large energy barrier. Such oxygen vacancies at the interface may play as charge-trapping sites, affecting the long-term device instability.

1 Introduction Since the demonstration of amorphous $InGaZnO_4$ (a-IGZO) with high mobility and good uniformity [1], amorphous semiconducting oxides (ASOs) become promising materials to be used in thin-film transistors (TFTs) for high performance electronics [2, 3]. However, various types of instabilities occur during the operation of ASO-based TFTs and this becomes a serious hurdle against the commercialization [3–5]. Most notably, the threshold voltage (V_T) significantly shifts negatively when the device is under the negative-bias-and-illumination stress (NBIS) [6, 7]. In resolving the instability issues, the first step would be the sound understanding of the phenomena by clarifying the atomistic origin causing the instability.

Numerous mechanisms [5, 8–12] were proposed to explain the NBIS problem. The early experiments were found to be strongly influenced by the environmental factors affecting the surface states of ASOs [8]. With the passivation layer protecting the device, the external effects could be excluded [8, 9], and a growing body of the research has focused on the intrinsic origin in ASO. Theoretically, defects such as peroxides (O_2^{2-}) [5], oxygen interstitial (O_i) [10], and oxygen vacancy (V_O) [11] were noted as the microscopic identities that cause the negative shift of V_T when they capture positive charges. On the other hand, several papers indicated that the NBIS instability is caused by the accumulation of positive charges at the interface between ASO and the gate dielectric (amorphous SiO_2 or a-SiO_2) since the negative gate bias attract the positive charges such as the photo-generated holes and V_O^+/V_O^{2+} to the interface [11–14]. The positive charges at the interface shift V_T by influencing the electrostatic potential in the ASO channel layer, leading to the negative shift of V_T. However, the microscopic structure of hole-trapping centers has not been revealed yet. In this regard, the *ab initio* modeling of the interface structure between ASO and a-SiO_2 is in high demands. Nevertheless, the theoretical study on the interface between ASO and a-SiO_2 has not been carried out yet to the best of our knowledge. In fact, the atomistic modeling of interfaces between *amorphous* materials is very rare [15].

In this paper, we carry out *ab initio* density-functional-theory calculations on amorphous IGZO–SiO_2 interface. First, we deliberately construct the interface model that is

energetically stable by satisfying chemical rules locally. The evaluated band offset between a-SiO_2 and a-IGZO agrees well with experiment. It is found that stoichiometric interface does not possess the deep trap centers. We also introduce V_O at various sites and find that Si and cations form bonds and generate deep levels that can hold holes. We suggest that these defect types can constitute the hole trapping site causing the instability under NBIS.

2 Computational details and modeling methods

Throughout this work, we use the Vienna *ab initio* simulation package (VASP) [16]. The projector augmented wave (PAW) pseudopotentials [17], the plane wave basis set with a kinetic energy cutoff of 500 eV, and a $3\times3\times1$ **k**-point mesh were used for electronic structure calculations. Regarding the pseudization scheme, Zn-d levels are included in the valence electrons while In- and Ga-d states are considered as core because they lie 8 eV below the bottom of oxygen p bands. For the exchange-correlation functional, we employ two types of functional. During the molecular dynamics (MD) simulations for obtaining the amorphous and interfacial structures, we use the PBEsol functional [18, 19], because it gives the most consistent bond lengths in crystalline structures of In_2O_3, Ga_2O_3, ZnO, and SiO_2 among the tested semi-local functionals. When investigating the electronic structures, we switch the exchange-correlation functional to the generalized gradient approximation plus U (GGA + U) functional [20] or hybrid functional of the Heyd–Scuseria–Ernzerhof (HSE) type [21, 22] with the screening parameter of 0.2 $Å^{-1}$ [23]. We choose the U value for the Zn-d orbitals as 7.5 eV in GGA + U to fit the energy positions of metal d orbitals to the photoemission data [24] and the mixing ratio of the exact exchange term in HSE (0.32) is determined to fit the band gap of crystalline IGZO.

In order to construct the interfacial structure, we first generate a-IGZO and a-SiO_2 through the independent melt-quench processes. The 126- and 96-atom cubic supercells with the fixed lattice constant of 11.45 Å are used for both a-IGZO and a-SiO_2, corresponding to the amorphous densities of 6.25 and 2.17 g cm^{-3}, respectively. These values correspond to the theoretical density of each amorphous structure when GGA + U functional is used, and they are close to the experimental values of 6.1 [25] and 2.20 g cm^{-3} [26], respectively. We employ the identical supercell geometry for the convenience of forming the interface structure. The melt-quench simulations are performed by pre-melting for 2 ps at 5000 K, melting for 15 (a-IGZO) and 10 (a-SiO_2) ps at 2500 K, and quenching to 300 K with a constant cooling rate of -250 K ps^{-1} [27, 28]. Then, the structures are relaxed until the atomic force is reduced to within 0.05 eV $Å^{-1}$.

Next, the cubic cells of a-IGZO and a-SiO_2 are sliced perpendicular to the z-axis, and joined under the periodic boundary conditions. Numerous combinations are possible depending on the slicing position along the z-axis and the relative shift in the xy-plane. We choose six interface models that appear to have stable interfacial Si- or metal–oxygen bonds without homopolar bonds such as Si–metal or oxygen–oxygen bonds. The as-formed interface models are annealed at 2000 K for 4 ps followed by quenching to 300 K with the cooling rate of -500 K ps^{-1}. During the annealing stage, some atoms diffuse by several Å but the intermixing of the two materials was not observed. Finally, the whole structures (including cell parameters) are fully relaxed at 0 K (the cell volume expanded by 2–3%). Figure 1 shows one of the final interface models.

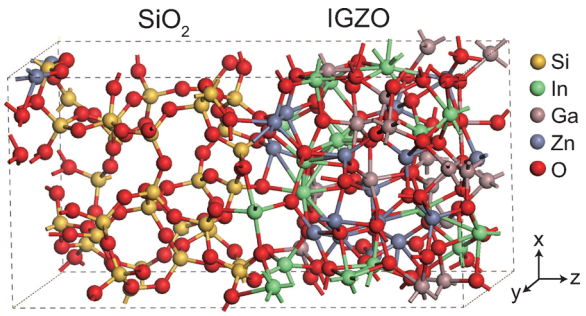

Figure 1 A representative of amorphous IGZO–SiO_2 interface model.

3 Results and discussion

3.1 Analysis on interface properties It is found that all of the interface models have no homopolar or metal–Si bonds at the interface, indicating that the two amorphous materials are chemically well connected. Every interfacial oxygen atom bridges Si and metal atoms with the coordination number of 2 or 3. The average In–O and Ga–O bond lengths at the interface (2.08 and 1.80 Å, respectively) are slightly shorter than the corresponding bulk values by ~0.1 Å, while the Si–O and Zn–O bond lengths are almost identical (1.63 and 1.98 Å, respectively). We could not identify any preference of cations at the interface as In, Ga, and Zn atoms are equally bonded to interfacial oxygen atoms.

In order to examine the stability of the interface, we calculate the interface energy (E_{int}) as follows:

$$E_{int}=\frac{1}{2}\left[E_{tot}(\text{interface})-E_{tot}(\text{a-IGZO})-E_{tot}(\text{a-SiO}_2)\right], \quad (1)$$

where E_{tot} is the total energy of the given system computed within the GGA + U functional. The averaged E_{int} is 12.4 meV $Å^{-2}$ which is on the same order of E_{int} of 6.8 meV $Å^{-2}$ between crystalline Si and a-SiO_2 [29], supporting the stability of the present interface models.

Another important property of the interface is the band offset. Typically, the theoretical band offset is evaluated using the macroscopically averaged potential for the interface between crystalline structures [30]. However, this is not feasible in the amorphous structure due to the lack of lattice periodicity. To obtain the reference points to line up the band structure, we first define the average oxygen 2s level for the

ith oxygen atom as follows:

$$E^i_{2s}=\frac{\int_{-\infty}^{E_F}(\epsilon - E_F)D^i_{2s}(\epsilon)d\epsilon}{\int_{-\infty}^{E_F} D^i_{2s}(\epsilon)d\epsilon}, \quad (2)$$

where $D^i_{2s}(\epsilon)$ is the partial density states of 2s orbital of the ith oxygen atom. Then, the macroscopic average of the oxygen 2s level is evaluated as follows:

$$\bar{E}_{2s}(z)=\frac{1}{2\lambda}\int_{z-\lambda}^{z+\lambda} dz' \int_0^{L_x} dx' \int_0^{L_y} dy' \sum_i^{N_O} E^i_{2s}\delta(\mathbf{r}' - \mathbf{r}_i), \quad (3)$$

where N_O is the total number of oxygen atoms within the supercell and $\mathbf{r}_i$ is the position of the ith oxygen atom. In this part, we employ the hybrid functional to match the band gap to the experimental value.

Figure 2a shows $\bar{E}_{2s}(z)$ with $\lambda = 1$ Å. It is found that $\bar{E}_{2s}(z)$ plateaus in the bulk region, allowing for determining the difference of the oxygen 2s levels between a-IGZO and a-SiO_2 to be 1.97 eV. Next, we compute the bulk structure of a-IGZO and a-SiO_2 using the same hybrid functional and evaluate the energy difference between the average oxygen 2s level and the valence band top, which is used in band line-up on top of the average oxygen 2s level. This gives the band offset of 1.2 eV that is in reasonable agreement with 1.43 eV measured by photoemission experiment [31]. On the other hand, it is well known that the structural disorder in the amorphous phase induce the localized tail states near the band edges. From the analysis on the inverse participation ratio, we find that the tail states are formed within 0.28 and 0.45 eV from the valence band top of a-SiO_2 and a-IGZO, respectively. When this is considered into the band alignment, the valence band offset is increased to 1.37 eV (see Fig. 2a).

Figure 2b shows the partial density of states that is spatially resolved along the interface normal direction. It is found that no localized state is formed within the band gap, which is also the case for other interface models. This means that the stoichiometric interface with stable chemical bonds do not have intrinsic trap levels that possibly capture holes.

3.2 Oxygen vacancy In many previous works, V_O was regarded as the source of the instability [11, 12, 32, 33]. To examine this, we introduce one V_O by removing an oxygen atom from the interface models, and fully relax the atomic positions within GGA + U functional. For the statistical average, two interface models are selected and about 180 V_O configurations are studied. We first compute the formation energy of the neutral V_O (Ω_V) as follows:

$$\Omega_V = E_{tot}(V_O) - E_{tot}(\text{interface}) + \mu_O, \quad (4)$$

where $E_{tot}(V_O)$ is total energy of the interface model including V_O, and μ_O is the oxygen chemical potential. Here, μ_O is set to the half of the total energy of the oxygen molecule, corresponding to the oxygen-rich condition.

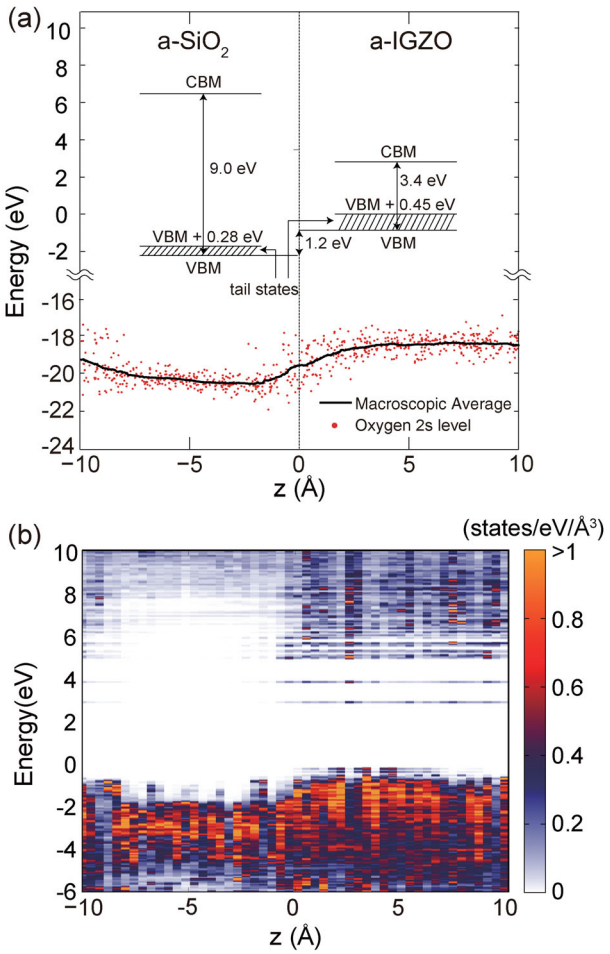

Figure 2 (a) The schematic diagram for the electronic structure of the constructed interface is shown. The calculated first-moment peaks for oxygen 2s level are plotted. The plateaus in the macroscopic average indicate the bulk regions of a-SiO_2 and a-IGZO. (b) Calculated partial density of states that is spatially resolved along the z-direction.

It has been well established that the formation energy of the shallow defect levels in semiconducting oxides suffers from the error caused by the band-gap underestimation and large dispersion in the conduction bands [34]. In order to reduce errors in Ω_V for the shallow defect state, we first determine the nature of each defect by examining its band dispersion and spatial distribution. For the oxygen vacancy concluded to be shallow in nature, we correct Ω_V by adding the band-gap error in GGA + U results.

Figure 3 shows the calculated Ω_V with respect to the z-position of V_O. The V_O's can be classified into four types according to the neighboring cations and deep/shallow characters: (i) deep V_O with Si–Si bond (V_O[Si–Si]), (ii) deep V_O with metal–metal bond (V_O[M–M]; M = In, Ga, or Zn) or (iii) shallow V_O with the broken metal bond (V_O[M···M]), and (iv) deep V_O with metal–Si bond (V_O[M–Si]). The com-

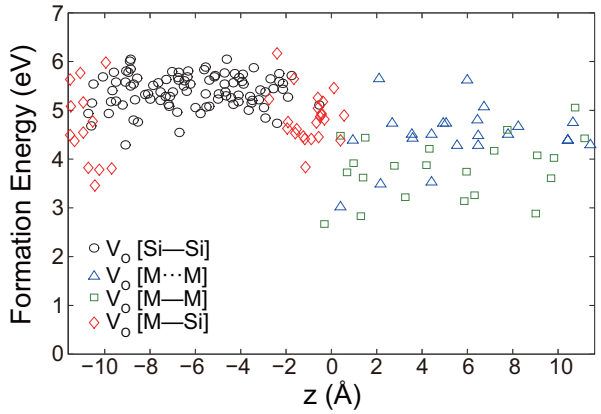

Figure 3 The formation energy of the neutral oxygen vacancy is shown with respect to the z-coordination. The vacancies are classified into four types according to neighboring cations.

puted Ω_V's inside the bulk region of a-SiO_2 and a-IGZO are in reasonable agreement with other works [27, 35, 36].

In Fig. 3, it is noteworthy that the deep levels are formed for many V_O's at the interface and they are accompanied by the metal–Si bonds. Figure 4a shows the detailed atomic configuration and local density of states. A dashed circle in Fig. 4a confirms that the localized defect level is developed at the interface. As shown in the right figure, it is found that most of this state (more than 70%) is distributed over Si, metal, and surrounding oxygen atoms. Since two electrons occupy this state, the interfacial V_O can play as hole-trapping sites.

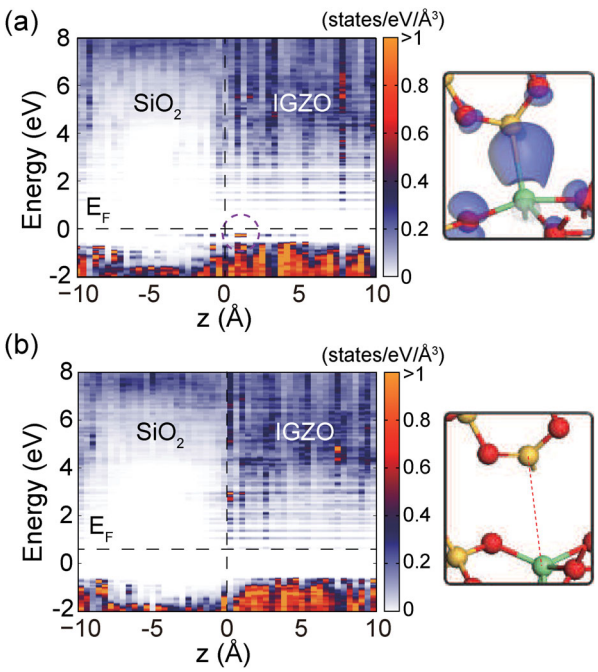

Figure 4 The local densities of states and atomic structures of (a) deep V_O[M–Si] and (b) resonant V_O[M···Si] are shown. The isosurface of the charge density of the defect state marked by the dashed circle in (a) is shown in the right. The isovalue is 3.4×10^{-3} e Å^{-3}.

The hole trapping into the deep interfacial V_O can be mimicked by removing two electrons from the supercell. Figure 4b shows the relaxed geometry and the corresponding electronic structure for V_O^{2+}[M–Si]. It is noticeable that the bond length of $[M\cdots Si]^{2+}$ is significantly elongated from 2.45 to 4.24 Å. Concurrently, the localized level with the band gap shifts into the conduction band and becomes a resonant state. We find that most interfacial V_O[M–Si]'s undergo similar deep-to-resonant transition upon hole trapping.

Based on the above V_O[M–Si], we propose a microscopic mechanism of the NBIS instability. First, the interfacial V_O[M–Si] could be generated during the growth process. Although V_O[M–Si] is less stable than V_O in a-IGZO bulk on average (see Fig. 3), the non-equilibrium condition may allow for the substantial generation of V_O[M–Si]. Furthermore, under the NBIS condition, ionized V_O^{2+} can electromigrate and accumulate at the interface. At the same time, the photo-excited holes in the channel layer will drift to the interface between the a-IGZO channel and a-SiO_2. Then, the holes will be captured by V_O[M–Si], followed by the deep-to-resonant transition from V_O[M–Si] to $V_O^{2+}[M\cdots Si]$. When NBIS is off, the captured holes would recombine with electrons if the energy barrier from Fig. 4b to Fig. 4a is overcome by thermal fluctuation. Even though we were not able to calculate the recovery barrier since the transition path is too complex, the large structural change in $V_O^{2+}[M\cdots Si]$ strongly suggests that the barrier should be significantly higher than for V_O^{2+} in the bulk region of a-IGZO. Therefore, we suggest that the V_O[M–Si] at the interface can contribute to the long-term negative shift of V_T in TFTs.

4 Summary In summary, to identify the source of charge trapping sites causing the device instability, we carried out *ab initio* calculations on the interface between a-SiO_2 and a-$InGaZnO_4$. The interface structure was modeled by carefully joining the two amorphous phases such that interface bonds between oxygen and Si/metal atoms were fully formed. The band offset was computed by aligning the oxygen 2s level and shows good agreement with experiment. For the stoichiometric interface, we could not find any charge trap levels within the band gap. This suggests that the clean interface without charge trapping sites can be synthesized in experiment. On the other hand, when V_O was introduced at the interface, the Si–metal bonds were formed together with the deep defect levels (V_O[M–Si]). We simulated the hole trapping into this defect by removing two electrons and it was found that the local structure near the Si–metal bond undergo a large relaxation. This implies that the recovery to the original neutral state would involve a large energy barrier. We believe that this is one of the main origin of the long-term stability issue in a-IGZO-based TFTs. The present results are also consistent with the recent experiment demonstrating the improvement in NBIS stability when the thermal annealing reduced the density of interfacial V_O [13].

Acknowledgements This work was supported by IBS-R009-D1, Samsung Display and the EDISON Program through the National Research Foundation of Korea (NRF) funded by the Ministry of Science, ICT & Future Planning (NRF-2012M3C1A6035307). The computations were carried out at KISTI supercomputing center (KSC-2014-C3-012).

References

[1] K. Nomura, H. Ohta, A. Takagi, T. Kamiya, M. Hirano, and H. Hosono, Nature **432**, 488 (2004).
[2] T. Kamiya and H. Hosono, NPG Asia Mater. **2**, 15 (2010).
[3] T. Kamiya, K. Nomura, and H. Hosono, Sci. Technol. Adv. Mater. **11**, 044305 (2010).
[4] H. Y. Jung, Y. Kang, A. Y. Hwang, C. K. Lee, S. Han, D.-H. Kim, J.-U. Bae, W.-S. Shin, and J. K. Jeong, Sci. Rep. **4**, 3765 (2014)
[5] H.-H. Nahm, Y.-S. Kim, and D. H. Kim, Phys. Status Solidi B **249**, 1277 (2012).
[6] M. D. H. Chowdhury, P. Migliorato, and J. Jang, Appl. Phys. Lett. **97**, 173506 (2010).
[7] K. H. Ji, J.-I. Kim, H. Y. Jung, S. Y. Park, R. Choi, U. K. Kim, C. S. Hwang, D. Lee, H. Hwang, and J. K. Jeong, Appl. Phys. Lett. **98**, 103509 (2011).
[8] J. K. Jeong, H. W. Yang, J. H. Jeong, Y.-G. Mo, and H. D. Kim, Appl. Phys. Lett. **93**, 123508 (2008).
[9] K. Nomura, T. Kamiya, and H. Hosono, Appl. Phys. Lett. **99**, 053505 (2011).
[10] J. Robertson and Y. Guo, Appl. Phys. Lett. **104**, 162102 (2014).
[11] B. Ryu, H.-K. Noh, E.-A. Choi, and K. J. Chang, Appl. Phys. Lett. **97**, 022108 (2010).
[12] J.-Y. Kwon, J. S. Jung, K. S. Son, K.-H. Lee, J. S. Park, T. S. Kim, J.-S. Park, R. Choi, J. K. Jeong, B. Koo, and S. Y. Lee, Appl. Phys. Lett. **97**, 183503 (2010).
[13] M. D. H. Chowdhury, J. G. Um, and J. Jang, Appl. Phys. Lett. **105**, 233504 (2014).
[14] H. Oh, S.-M. Yoon, M. K. Ryu, C.-S. Hwang, S. Yang, and S.-H. K. Park, Appl. Phys. Lett. **98**, 033504 (2011).
[15] P. Broqvist, A. Alkauskas, J. Godet, and A. Pasquarello, J. Appl. Phys. **105**, 061603 (2009).
[16] G. Kresse and J. Hafner, Phys. Rev. B **47**, 558 (1993).
[17] P. E. Blöchl, Phys. Rev. B **50**, 17953 (1994).
[18] J. P. Perdew, A. Ruzsinszky, G. I. Csonka, O. A. Vydrov, G. E. Scuseria, L. A. Constantin, X. Zhou, and K. Burke, Phys. Rev. Lett. **100**, 136406 (2008).
[19] J. P. Perdew, K. Burke, and M. Ernzerhof, Phys. Rev. Lett. **77**, 3865 (1996).
[20] S. L. Dudarev, G. A. Botton, S. Y. Savrasov, C. J. Humphreys, and A. P. Sutton, Phys. Rev. B **57**, 1505 (1998).
[21] J. Heyd, G. E. Scuseria, and M. Ernzerhof, J. Chem. Phys. **118**, 8207 (2003).
[22] J. Heyd, G. E. Scuseria, and M. Ernzerhof, J. Chem. Phys. **124**, 219906 (2006).
[23] A. V. Krukau, O. A. Vydrov, A. F. Izmaylov, and G. E. Scuseria, J. Chem. Phys. **125**, 224106 (2006).
[24] K. Nomura, T. Kamiya, E. Ikenaga, H. Yanagi, K. Kobayashi, and H. Hosono, J. Appl. Phys. **109**, 073726 (2011).
[25] A. Hino, S. Kosaka, S. Morita, S. Yasuno, T. Kishi, K. Hayashi, and T. Kugimiya, ECS Solid State Lett. **1**, Q51 (2012).
[26] A. Pasquarello and R. Car, Phys. Rev. Lett. **79**, 1766 (1997).
[27] H.-K. Noh, K. J. Chang, B. Ryu, and W.-J. Lee, Phys. Rev. B **84**, 115205 (2011).
[28] Y. J. Oh, H.-K. Noh, and K. J. Chang, Physica B **407**, 2989 (2012).
[29] Y. Tu and J. Tersoff, Phys. Rev. Lett. **84**, 4393 (2000).
[30] W.-J. Son, E. Cho, B. Lee, J. Lee, and S. Han, Phys. Rev. B **79**, 245411 (2009).
[31] E. A. Douglas, A. Scheurmann, R. P. Davies, B. P. Gila, H. Cho, V. Craciun, E. S. Lambers, S. J. Pearton, and F. Ren, Appl. Phys. Lett. **98**, 242110 (2011).
[32] Y. Jeong, C. Bae, D. Kim, K. Song, K. Woo, H. Shin, G. Cao, and J. Moon, Appl. Mater. Interfaces **2**, 611 (2011).
[33] Y.-G. Lee and W.-S. Choi, Electron. Mater. Lett. **9**, 719 (2013).
[34] W.-J. Yin, J. Ma, S.-H. Wei, M. M. Al-Jassim, and Y. Yan, Phys. Rev. B **86**, 045211 (2012).
[35] T. Tamura, G.-H. Lu, and R. Yamamoto, Phys. Rev. B **69**, 195204 (2004)
[36] T. Kamiya, K. Nomura, and H. Hosono, Phys. Status Solidi A **207**, 1698 (2010).

